



**HAL**  
open science

## Ultracold Dipolar Molecules Composed of Strongly Magnetic Atoms

A. Frisch, M. Mark, K. Aikawa, S. Baier, R. Grimm, A. Petrov, S. Kotochigova, Goulven Quéméner, Maxence Lepers, Olivier Dulieu, et al.

► **To cite this version:**

A. Frisch, M. Mark, K. Aikawa, S. Baier, R. Grimm, et al.. Ultracold Dipolar Molecules Composed of Strongly Magnetic Atoms. *Physical Review Letters*, 2015, 115 (20), pp.203201. 10.1103/PhysRevLett.115.203201 . hal-04576660

**HAL Id: hal-04576660**

**<https://hal.science/hal-04576660v1>**

Submitted on 17 May 2024

**HAL** is a multi-disciplinary open access archive for the deposit and dissemination of scientific research documents, whether they are published or not. The documents may come from teaching and research institutions in France or abroad, or from public or private research centers.

L'archive ouverte pluridisciplinaire **HAL**, est destinée au dépôt et à la diffusion de documents scientifiques de niveau recherche, publiés ou non, émanant des établissements d'enseignement et de recherche français ou étrangers, des laboratoires publics ou privés.

# Ultracold polar molecules composed of strongly magnetic atoms

A. Frisch,<sup>1,2</sup> M. Mark,<sup>1</sup> K. Aikawa,<sup>1,\*</sup> S. Baier,<sup>1</sup> R. Grimm,<sup>1,2</sup> A. Petrov,<sup>3,†</sup>  
S. Kotochigova,<sup>3</sup> G. Quémener,<sup>4</sup> M. Lepers,<sup>4</sup> O. Dulieu,<sup>4</sup> and F. Ferlaino<sup>1,2</sup>

<sup>1</sup>*Institut für Experimentalphysik und Zentrum für Quantenphysik,  
Universität Innsbruck, Technikerstrasse 25, 6020 Innsbruck, Austria*

<sup>2</sup>*Institut für Quantenoptik und Quanteninformation,  
Österreichische Akademie der Wissenschaften, 6020 Innsbruck, Austria*

<sup>3</sup>*Department of Physics, Temple University, Philadelphia, Pennsylvania 19122, USA*

<sup>4</sup>*Laboratoire Aimé Cotton, CNRS, Université Paris-Sud, ENS Cachan, 91405 Orsay, France*

(Dated: April 20, 2015)

In a combined experimental and theoretical effort, we demonstrate a novel type of dipolar system made of ultracold bosonic polar molecules with large magnetic dipole moments. Our polar molecules are formed in weakly bound Feshbach molecular states from a sample of strongly magnetic bosonic erbium atoms. We show that the ultracold magnetic molecules can carry very large dipole moments and we demonstrate how to create and characterize them, and how to change their orientation. Finally, we confirm that the relaxation rates of molecules in a quasi-two dimensional geometry can be reduced by using the anisotropy of the dipole-dipole interaction and that this reduction follows a universal dipolar behavior.

PACS numbers: 34.50.-s, 31.10.+z, 34.50.Cx

Ultracold dipolar particles are at the heart of very intense research activities, which aim to study the effect of interactions that are anisotropic and long range [1, 2]. Dipolar quantum phenomena require ultracold gases and a strong dipole-dipole interaction (DDI). So far, strongly dipolar gases have been obtained using either atoms with a large magnetic dipole moment or ground-state polar molecules with an electric dipole moment [2]. With both systems, many fascinating many-body quantum effects have been observed and studied, such as the  $d$ -wave collapse of a dipolar Bose-Einstein condensate [3], the deformation of the Fermi sphere [4], and the spin-exchange phenomena [5, 6].

Here, we introduce a novel kind of strongly dipolar particles. These are weakly bound polar molecules produced from atoms with large magnetic dipole moments, such as erbium (Er) and other lanthanides. The key point is that these molecules can have a very large magnetic moment  $\mu$  up to twice that of atoms (e.g. 14 Bohr magneton,  $\mu_B$ , for  $\text{Er}_2$ ) and have twice the mass of the atoms. As a consequence, the degree of “dipolarity” of the magnetic molecules is much larger than the one of atoms. This can be quantified in terms of the dipolar length  $a_d = m\mu_0\mu^2/(4\pi\hbar^2)$  [1], which characterizes the length of the DDI and solely depends on the molecular mass  $m$  and on  $\mu$ ;  $\hbar$  is the Planck constant divided by  $2\pi$ . For instance,  $\text{Er}_2$  with  $\mu = 14\mu_B$  has  $a_d \approx 1600a_0$ , with  $a_0$  being Bohr’s radius. Moreover, in contrast to ground-state heteronuclear molecules, the dipole moment of the magnetic molecules is permanent, opening the possibility of investigating the physics of unpolarized dipoles at zero external (magnetic) field.

In a combined experimental and theoretical effort, we produce and study ultracold  $\text{Er}_2$  polar molecules. Er-

bium is a sub-merged shell lanthanide with a large magnetic moment and a large orbital angular momentum quantum number,  $L = 5$ . This species, like other magnetic lanthanides [7–9], exhibits anisotropic interactions at both long and short ranges. These interactions are the long-range magnetic DDI and the short-range anisotropic van der Waals (vdW) interaction coming from the non-zero value of  $L$  [10, 11]. As a consequence, magnetic lanthanides possess extraordinary dense spectra of Feshbach resonances as demonstrated in recent scattering experiments [12–14]. Each resonance position marks an avoided crossing between the atomic scattering threshold and a molecular bound state. The avoided crossing can be used to associate molecules from atom pairs [15].

We create and probe  $\text{Er}_2$  polar molecules by using standard magneto-association and imaging techniques [15]. Details of the production schemes are described in the Supplemental Material [16]. In brief, we begin with an ultracold sample of  $^{168}\text{Er}$  atoms in an optical dipole trap (ODT) in a crossed-beam configuration. The atoms are spin-polarized into the lowest Zeeman sublevel ( $j = 6$ ,  $m_j = -6$ ). Here,  $j$  is the atomic electronic angular momentum quantum number and  $m_j$  is its projection on the quantization axis along the magnetic field. To associate  $\text{Er}_2$  molecules, we ramp the magnetic field across one of the low-field Feshbach resonances observed in Er [12, 13]. We experimentally optimize the ramping parameters, such as the ramp speed and the magnetic-field sweep interval, by maximizing the conversion efficiency. In our experiment we typically achieve a conversion efficiency of 15%, which is a common value for boson-composed Feshbach molecules [15]. To obtain a pure molecular sample, we remove all the remaining atoms from the ODT by applying a resonant laser pulse. Our final molecular

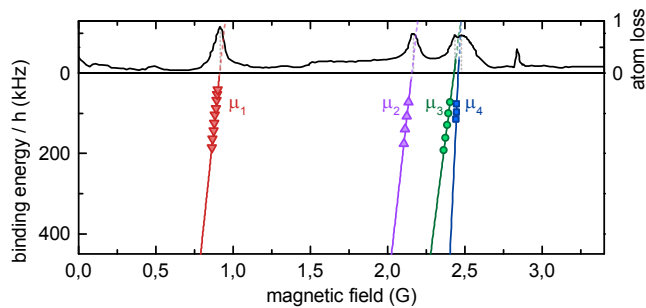


Figure 1. Er<sub>2</sub> weakly bound molecules. (a) Atom-loss spectrum [12] from 0 to 3 G and (b) near-threshold binding energy of the corresponding molecular states. The solid lines are fit to the experimental data and extrapolated to larger  $E_b$  up to  $h \times 500$  kHz. The error bars are smaller than the symbols.

sample contains about  $2 \times 10^4$  Er<sub>2</sub> Feshbach molecules at a temperature of 300 nK and at a density of about  $8 \times 10^{11} \text{ cm}^{-3}$  [16].

A first central question regards the magnitude of the dipole moment owned by the magnetic molecules. We experimentally determine  $\mu$  by using magnetic-field modulation spectroscopy, a technique which was successfully applied to alkali atoms [17–19]. With this method, we measure the molecular binding energy  $E_b$  as a function of  $B$  near the atomic threshold, and we extract  $\mu$  by using the relation  $\mu \equiv 2\mu_a - |dE_b(B)/dB|$ . Our spectroscopic measurement begins with an ultracold atomic sample near a Feshbach resonance. We then add a small sinusoidal modulation to the bias magnetic field for 400 ms. The modulation frequency is varied at each experimental run. When it matches  $E_b/h$ , prominent atom losses appear because of molecule formation. We trace the near-threshold molecular spectrum by repeating the measurement for various magnetic-field values.

As shown in Fig. 1, we focus on four molecular energy levels, which near threshold exhibit a linear dependence on  $B$ . Each state has a different  $\mu$ , ranging from 8 to  $12 \mu_B$ , as listed in Table I. We point out that the present investigation is restricted to magnetic field values up to 3 G. However, the extraordinarily dense spectrum of Feshbach resonances observed in Er [13] reflects an equally dense and rich molecular energy spectrum, opening the exciting prospect of cruising through molecular states of different magnetic moments or creating molecular-state mixtures [19–21]. For future experiments, it will be very interesting to access molecular levels parallel to the atomic threshold for which  $\mu = 2\mu_a$  [19].

Prior to this work, the Er<sub>2</sub> molecular energy structure near the threshold was unknown. Given the complex scattering physics involving highly anisotropic interactions and many partial waves [13], conventional theoretical approaches based on coupled-channel calculations, which have been so successful in reproducing the scatter-

Table I. Experimental and theoretical magnetic moments of four molecular states near the atomic threshold, Feshbach-resonance positions  $B_{\text{FR}}$ , dipolar lengths, outer turning points  $R^*$ , and dominant quantum numbers  $\ell$ ,  $J$ , and  $M$ . For convenience, the molecular states are labeled as  $\mu_i$  with  $i = 1, \dots, 4$ . The error is one standard deviation of the statistical error.

	$B_{\text{FR}}$ (G)	$\mu$ ( $\mu_B$ )		$a_d$ ( $a_0$ )	$R^*$ ( $a_0$ )	$ \ell, J, M\rangle$
		Exp.	Theo.			
$\mu_1$	0.91	11.30(7)	11.20	1041(13)	72.0	$ 4, 12, -12/-10/-9\rangle$
$\mu_2$	2.16	11.51(4)	11.46	1080(8)	71.0	$ 4, 10, -10\rangle$
$\mu_3$	2.44	11.84(2)	11.75	1143(4)	86.0	$ 2, 12, -10\rangle$
$\mu_4$	2.47	7.96(3)	7.92	517(4)	57.0	$ 6, 10, -7/-6\rangle$

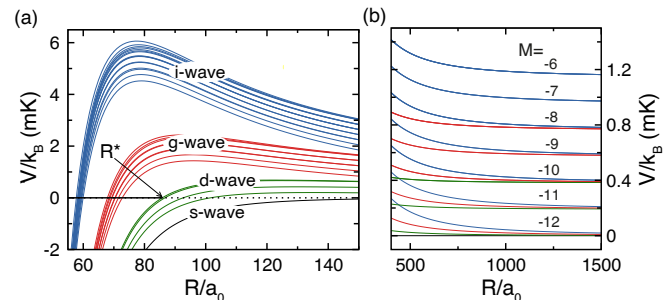


Figure 2. Adiabatic interaction potentials of two Er atoms at medium- (a) and long- (b) interatomic separation  $R$ . The calculation is performed at  $B = 2.44$  G with  $m_\ell + M = -12$  and includes only states with even  $\ell \leq 6$ . The zero of energy is at the dissociation limit of two  $|j, m\rangle = |6, -6\rangle$  atoms. Black, green, red, and blue curves indicate the dominant  $\ell$ -wave character. The horizontal black line indicates a  $d$ -wave Feshbach molecule with an outer turning point  $R = R^*$  resonant with the  $s$ -wave entrance channel. Panel (b) also shows the  $M$  projection for each of the Zeeman dissociation limit.

ing resonances and the molecular spectra for alkali-metal atoms [15], are yet out of reach for magnetic lanthanides. To gain insight into the molecular spectrum and scattering physics of such an anisotropic species, we develop a new theoretical model based on approximate adiabatic potentials. Our model, which is inspired by work on alkali-metal collisions [22–25], uses the measured values of  $\mu$  and of the resonance positions as input parameters. With this combined experimental and theoretical approach, we are able to reach an assignment of the dominant molecular quantum numbers  $\ell$ ,  $J$ , and  $M$  for the above investigated states.

In our model, the Feshbach resonances are related to weakly bound vibrational states of the adiabatic potentials  $U_n(R; B)$ ,  $n = 1, 2, \dots$ . The potentials  $U_n(R; B)$  are the eigenvalues of the atom-atom interaction potential operator at given  $B$  and interatomic separation  $R$ . At large  $R$ , the interaction is given by the DDI and the isotropic and anisotropic van-der-Waals dispersion interactions. Details of our theoretical approach are described in the Supplemental Material [16]. Figure 2 shows  $U_n(R; B)$  calculated at  $B = 2.44$  G. We distinguish four

groups of potentials, each associated with a dominant partial wave  $\ell$ . Within a group, the potentials are split by the Zeeman energy and the magnetic DDI and dissociate at a different atomic thresholds. For each potential  $U_n(R; B)$  we can further assign the dominant  $J$  and  $M$ , where  $\vec{J} = \vec{j}_1 + \vec{j}_2$  is the sum of electronic angular momenta of two atoms and  $M$  is the projection of  $J$  on the internuclear axis. The figure also shows an example of predominantly  $d$ -wave Feshbach molecules with an outer classical turning point  $R^*$ . Its “adiabatic” molecular magnetic moment is to good approximation given by  $\mu^{\text{calc}} \approx -dU_n(R^*; B)/dB$ , where we further use that most of the vibrational wavefunction is localized around  $R^*$ . Interestingly, we observe that the  $\mu^{\text{calc}}$  value quickly converges with the number of included  $\ell$  (even  $\ell \leq 6$  is sufficient) and that it strongly depends on the DDI but only weakly on the vdW dispersion potential. In fact, at  $R^*$  the DDI dominates over the anisotropic part of the dispersion potential.

Finally, we assume for each Feshbach resonance a vibrational state that is on resonance and then find the adiabatic potential which has a magnetic moment closest to the measured one within 1%. Once the best matching is identified, the corresponding  $U_n(R; B)$  sets the dominant molecular quantum numbers  $\ell$ ,  $J$ , and  $M$ . As summarized in Table I, in our range of investigation we observe  $d$ -,  $g$ -, and  $i$ -wave molecular states. These states show several dominant  $M$  contributions. This fact is unusual and reflects the dominant role of the DDI, which couples several adiabatic potentials and  $M$  components. This mixing effect is particularly dominant below 10 G, where the DDI at  $R^*$  is larger than the Zeeman interaction. Above 10 G, we predict  $\mu$  to be equal to integer multiples of  $g\mu_B$  [16], where  $g$  is the Er atomic Landé-factor.

As a consequence of the extremely large magnetic dipole moments of  $\text{Er}_2$ , the molecule behavior is expected to be dominated by the DDI; see Table I. For instance,  $\text{Er}_2$  with the largest measured  $\mu$  value possesses  $a_d \approx 1150 a_0$ . Remarkably, this value is comparable to the one realized with ground-state KRb molecules [26], which are an extensively investigated case and can thus serve as a benchmark dipolar system. From a comparative analysis between  $\text{Er}_2$  and KRb, one can unveil universal marks imprinted by the DDI, especially given that the two systems are very different in nature, yet sharing a similar degree of dipolarity. Their profound differences are clear:  $\text{Er}_2$  is a weakly bound homonuclear magnetic molecule in a highly excited vibrational levels, whereas KRb are deeply bound heteronuclear molecules in the absolute ground-state.

Following Refs. [27–29], we focus on the study of the collisional stability of  $\text{Er}_2$  both in a three- (3D) and in a quasi two-dimensional (q2D) trap for two different dipole orientations. The dipole orientation is controlled by changing the direction of the magnetic field and is represented by the angle  $\theta$  between the magnetic field axis

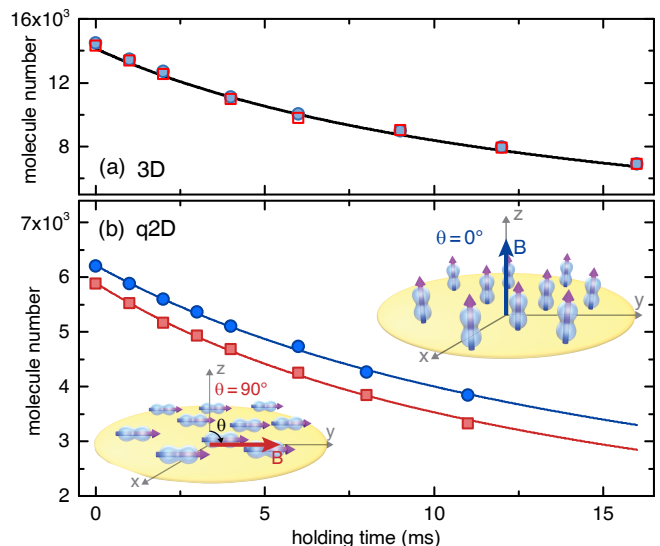


Figure 3. Typical time evolution of the number of molecules for  $\theta = 90^\circ$  (squares) and  $\theta = 0^\circ$  (circles) in a 3D (a) and in a q2D trap (b). The data refer to molecules in the state  $\mu_1$  for the 3D case (a) and molecules in the state  $\mu_2$  in q2D (b). The insets in (b) show an illustration of molecules in pancake-shaped traps with side-by-side (right) and head-to-tail (left) orientations. The solid lines are two-body decay fits to the data. The error bars for (a) and (b) are smaller than the data points and are not shown. We calculate the statistical error from averaging over 5 independent measurements in (a) and about 50 in (b).

and the gravity axis. Our experiment begins with the atomic sample trapped either in a 3D or in a q2D ODT. The q2D trap is created by superimposing a vertically oriented, one-dimensional optical lattice [16]. After the magneto-association and the removal of the remaining atoms, we probe the time evolution of the molecule number for head-to-tail ( $\theta = 90^\circ$ ) and side-by-side ( $\theta = 0^\circ$ ) dipole orientation. We extract the corresponding relaxation rate coefficients,  $\beta_\perp$  and  $\beta_\parallel$ , using a standard two-body rate equation [30].

Figure 3 shows typical molecular decay curves in (a) 3D and in (b) q2D. In 3D, we confirm that the inelastic decay does not depend on  $\theta$ . We obtain  $\beta_{3D} = 1.3(2) \times 10^{-10} \text{ cm}^3/\text{s}$ . This is a typical value for boson-composed Feshbach molecules, which undergo a rapid vibrational quenching into lower-lying molecular states, as demonstrated with alkali atoms [30]. Contrary, in q2D the decay rates clearly depend on the dipole orientation. We perform the decay measurements with molecules in state  $\mu_1$ ,  $\mu_2$ , and  $\mu_4$  [31]. For each molecular state,  $\beta_\perp$  is larger than  $\beta_\parallel$  with a reduction of losses up to 30% for side-by-side orientation, for which the DDI is predominantly repulsive, as compared to head-to-tail orientation. The ratio  $\frac{\beta_\perp(T)}{\beta_\parallel(T)}$  increases with increasing  $\mu$ ; see Table II.

The reduction of losses in q2D draws a natural analogy with the observations obtained with KRb molecules

Table II. Experimental and theoretical loss rate coefficients  $\beta$  for  $T = 400$  nK and for various  $\mu$  and  $\theta$  at  $B = 200$  mG. Uncertainties of  $\beta$  are statistical from fitting and systematic due to number density uncertainty. For the slightly different values of  $\mu$  compared to Table I and the error discussion see Supplemental Material [16].

	$\mu$ ( $\mu_B$ )	$\beta_{\perp}$ ( $10^{-6}$ cm <sup>2</sup> /s)		$\beta_{\parallel}$ ( $10^{-6}$ cm <sup>2</sup> /s)	
		Exp.	Theo.	Exp.	Theo.
$\mu_4$	8.7(6)	$12.5 \pm 0.3 \pm 3.3$	6.00	$10.6 \pm 0.3 \pm 2.8$	4.79
$\mu_1$	10.9(5)	$9.5 \pm 0.2 \pm 2.5$	6.81	$7.3 \pm 0.1 \pm 2.1$	5.07
$\mu_2$	11.7(3)	$11.3 \pm 0.2 \pm 2.9$	7.12	$8.6 \pm 0.2 \pm 2.3$	5.13

[29]. To get a quantitative comparison, we theoretically study the scattering behavior of Er<sub>2</sub> using the same formalism successfully employed for KRb. We compute the Er<sub>2</sub> + Er<sub>2</sub> loss rate coefficients  $\beta(T)$  in 3D and in q2D for given values of  $\mu$ ,  $\theta$ , and  $T$ . By averaging over a 3D and a 2D Maxwell-Boltzmann distribution, we obtain the thermalized loss rate coefficients  $\beta(T)$  in 3D and in q2D, respectively. The formalism accounts for the dominant long-range interactions at ultralow temperatures: the DDI and the isotropic vdW interaction [16].

In 3D, we find a rate coefficient of  $1.01 \times 10^{-10}$  cm<sup>3</sup>/s at  $T = 300$  nK, which is close to the experimental value [32]. In q2D, our calculations show that the collision dynamics at long range, and thus the value of  $\beta$ , depends on the dipole orientation and monotonically increases with  $\mu$ . In Table II, we compare theory and experiment and observe a good qualitative agreement. As in the experiments, our calculations show that head-to-tail collisions ( $\beta_{\perp}$ ) lead to larger molecular losses than side-by-side collisions ( $\beta_{\parallel}$ ). From a quantitative side, the absolute values of  $\beta$  differ by up to a factor of 2. This difference comes from the fact that our theoretical calculations do not include details of the short range physics since the Er<sub>4</sub> potential energy surfaces are currently unknown [16]. Then it is theoretically impossible to predict the absolute magnitude.

Remarkably, when comparing the theoretical and experimental values of the ratio  $\frac{\beta_{\perp}(T)}{\beta_{\parallel}(T)}$  of bosonic <sup>168</sup>Er<sub>2</sub> versus  $a_d/a_{\text{ho}}$  in Fig. 4, we observe good agreement as the ratio is determined by the DDI and not by the short-range physics [16]. Here,  $a_{\text{ho}}$  is the harmonic oscillator length along the tightly confining axis direction in q2D, given by  $\sqrt{\hbar/(2\pi\nu_z m)}$ , with trap frequency  $\nu_z$ . This suggests that despite the unknown short-range physics, we can correctly describe  $\frac{\beta_{\perp}(T)}{\beta_{\parallel}(T)}$  of Feshbach molecules using a point-like-dipole formalism. More generally, a simple analysis based on the universal behavior of dipolar collisions in confined systems [33] in the Wigner regime actually leads to the following universal scaling laws for the ratio [16]:  $\frac{\beta_{\perp}(T)}{\beta_{\parallel}(T)} \sim \left(\frac{a_{\text{dB}}}{a_{\text{ho}}}\right)^4 \frac{a_d}{a_{\text{ho}}} \exp\left[2\left(\frac{a_d}{a_{\text{ho}}}\right)^{2/5}\right]$  for bosons when  $a_d, a_{\text{ho}} > a_{\text{vdW}}$ , and  $\frac{\beta_{\perp}(T)}{\beta_{\parallel}(T)} \sim \left(\frac{a_d}{a_{\text{vdW}}}\right)^3$  for fermions when  $a_d, a_{\text{vdW}} < a_{\text{ho}}$ , with  $a_{\text{dB}} = h/\sqrt{2\pi m k_B T}$  the de

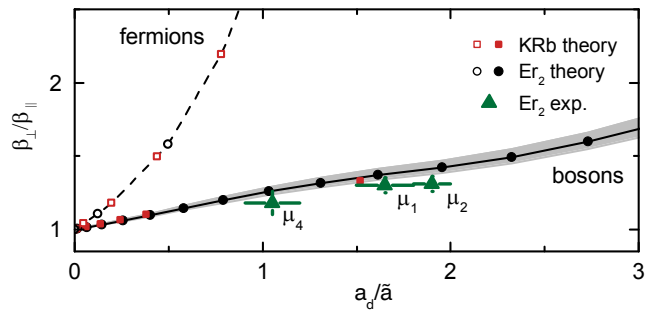


Figure 4. Universal loss rate ratio  $\beta_{\perp}/\beta_{\parallel}$  as a function of  $a_d/\tilde{a}$  for Er<sub>2</sub> (circles) and KRb (squares) for a fixed value  $a_{\text{dB}}/a_{\text{ho}} = 4.85$  corresponding to  $T = 400(40)$  nK and  $\nu_z = 31.2(1)$  kHz (see text). The gray shaded area is due to the uncertainty of  $T$ . Here,  $\tilde{a} = a_{\text{ho}}$  for bosonic molecules (filled symbols) and  $\tilde{a} = a_{\text{vdW}}$  for fermionic molecules (open symbols). The calculated loss rate ratios of Er<sub>2</sub> are compared with the experimental data for states  $\mu_1$ ,  $\mu_2$ , and  $\mu_4$  (triangles).

Broglie wavelength and  $a_{\text{vdW}} = (2mC_6/\hbar^2)^{1/4}$  the vdW length, and  $C_6$  the vdW coefficient. We confirm these universal behaviors by comparing the numerical results for bosonic <sup>41</sup>K<sup>87</sup>Rb and <sup>168</sup>Er<sub>2</sub>, and fermionic <sup>40</sup>K<sup>87</sup>Rb and <sup>167</sup>Er<sup>168</sup>Er; see Fig. 4. No matter the magnetic or electric dipolar system used, we find a unique universal curve for bosons as a function of  $a_d/a_{\text{ho}}$  and a unique one for fermions as a function  $a_d/a_{\text{vdW}}$ , as suggested by the analytical model. The faster increase of  $\frac{\beta_{\perp}(T)}{\beta_{\parallel}(T)}$  for fermions with respect to bosons is due to the statistical fermionic suppression of  $\beta_{\parallel}(T)$  in q2D that does not occur for bosons as explained in Ref. [34].

To conclude, our work demonstrates a simple way to create ultracold polar molecules where each individual atom carries a large magnetic dipole moment. We provide a clear signature of the dipolar character of the Er<sub>2</sub> molecules by performing scattering experiments in a q2D confinement, which is in good agreement with theoretical predictions. We anticipate that this system has the potential to open regimes of investigations, which have been inaccessible so far. In contrast to electric polar molecules, where the electric dipole moment is zero in the absence of a polarizing electric field, magnetic polar molecules have a permanent dipole moment allowing to study the physics of unpolarized dipoles. In addition, magnetic polar Feshbach molecules are diffuse in space with a typical size on the order of the vdW length. This novel situation can also have interesting consequences and trigger the development of extended scattering models, which account for multi-polar effects and truly four-body contributions when the molecule size becomes comparable to  $a_d$ . Finally, a very promising development will be to create fermionic Er<sub>2</sub> polar molecules where vibrational quenching processes are intrinsically suppressed because of the Pauli exclusion principle [35, 36].

This work is supported by the Austrian Ministry of

Science and Research (BMWF) and the Austrian Science Fund (FWF) through a START Grant under Project No. Y479-N20 and by the European Research Council under Project No. 259435. Research at Temple University is supported by an AFOSR grant No. FA9550-14-1-0321 and NSF grant No. PHY-1308573. G.Q., M.L. and O.D. acknowledge the financial support of “Projet Attractivité 2014” from Université Paris-Sud and the COPOMOL project (#ANR-13-IS04-0004) from Agence Nationale de la Recherche.

---

\* Current address: Department of Physics, Graduate School of Science and Engineering, Tokyo Institute of Technology, 2-12-1-S5-9, Ookayama, Meguro-ku, Tokyo 152-8551, Japan.

† Alternative address: NRC “Kurchatov Institute” PNPI 188300, Division of Quantum Mechanics, St. Petersburg State University, 198904, Russia.

- [1] M. A. Baranov, M. Dalmonte, G. Pupillo, and P. Zoller, *Chem. Rev.* **112**, 5012 (2012).
- [2] T. Lahaye, C. Menotti, L. Santos, M. Lewenstein, and T. Pfau, *Rep. Prog. Phys.* **72**, 126401 (2009).
- [3] T. Lahaye, T. Koch, B. Fröhlich, M. Fattori, J. Metz, A. Griesmaier, S. Giovanazzi, and T. Pfau, *Nature* **448**, 672 (2007).
- [4] K. Aikawa, S. Baier, A. Frisch, M. Mark, C. Ravensbergen, and F. Ferlaino, *Science* **345**, 1484 (2014).
- [5] B. Yan, S. A. Moses, B. Gadway, J. P. Covey, K. R. A. Hazzard, A. M. Rey, D. S. Jin, and J. Ye, *Nature* **501**, 521 (2013).
- [6] A. de Paz, A. Sharma, A. Chotia, E. Maréchal, J. H. Huckans, P. Pedri, L. Santos, O. Gorceix, L. Vernac, and B. Laburthe-Tolra, *Phys. Rev. Lett.* **111**, 185305 (2013).
- [7] M. Lu, N. Q. Burdick, S. H. Youn, and B. L. Lev, *Phys. Rev. Lett.* **107**, 190401 (2011).
- [8] D. Sukachev, A. Sokolov, K. Chebakov, A. Akimov, S. Kanorsky, N. Kolachevsky, and V. Sorokin, *Phys. Rev. A* **82**, 011405 (2010).
- [9] J. Miao, J. Hostetter, G. Stratis, and M. Saffman, *Phys. Rev. A* **89**, 041401 (2014).
- [10] A. Petrov, E. Tiesinga, and S. Kotochigova, *Phys. Rev. Lett.* **109**, 103002 (2012).
- [11] M. Lepers, J.-F. Wyart, and O. Dulieu, *Phys. Rev. A* **89**, 022505 (2014).
- [12] K. Aikawa, A. Frisch, M. Mark, S. Baier, A. Rietzler, R. Grimm, and F. Ferlaino, *Phys. Rev. Lett.* **108**, 210401 (2012).
- [13] A. Frisch, M. Mark, K. Aikawa, F. Ferlaino, J. L. Bohn, C. Makrides, A. Petrov, and S. Kotochigova, *Nature* **507**, 475 (2014).
- [14] K. Baumann, N. Q. Burdick, M. Lu, and B. L. Lev, *Phys. Rev. A* **89**, 020701 (2014).
- [15] C. Chin, R. Grimm, P. Julienne, and E. Tiesinga, *Rev. Mod. Phys.* **82**, 1225 (2010).
- [16] See the Supplemental Material at [URL will be inserted by publisher] for details regarding the creation of  $\text{Er}_2$  molecules, the theoretical description of the collision formalism, and the adiabatic model.
- [17] N. R. Claussen, S. J. J. M. F. Kokkelmans, S. T. Thompson, E. A. Donley, E. Hodby, and C. E. Wieman, *Phys. Rev. A* **67**, 060701 (2003).
- [18] S. T. Thompson, E. Hodby, and C. E. Wieman, *Phys. Rev. Lett.* **95**, 190404 (2005).
- [19] M. Mark, F. Ferlaino, S. Knoop, J. G. Danzl, T. Kraemer, C. Chin, H.-C. Nägerl, and R. Grimm, *Phys. Rev. A* **76**, 042514 (2007).
- [20] M. Mark, T. Kraemer, P. Waldburger, J. Herbig, C. Chin, H.-C. Nägerl, and R. Grimm, *Phys. Rev. Lett.* **99**, 113201 (2007), 10.1103/PhysRevLett.99.113201.
- [21] F. Lang, P. van der Straten, B. Brandstätter, G. Thalhammer, K. Winkler, P. S. Julienne, R. Grimm, and J. Hecker Denschlag, *Nature Phys.* **4**, 223 (2008).
- [22] A. J. Moerdijk, B. J. Verhaar, and A. Axelsson, *Phys. Rev. A* **51**, 4852 (1995).
- [23] C. A. Stan, M. W. Zwierlein, C. H. Schunck, S. M. F. Raupach, and W. Ketterle, *Phys. Rev. Lett.* **93**, 143001 (2004).
- [24] E. Wille, F. M. Spiegelhalter, G. Kerner, D. Naik, A. Trenkwalder, G. Hendl, F. Schreck, R. Grimm, T. G. Tiecke, J. T. M. Walraven, S. J. J. M. F. Kokkelmans, E. Tiesinga, and P. S. Julienne, *Phys. Rev. Lett.* **100**, 053201 (2008).
- [25] T. G. Tiecke, M. R. Goosen, J. T. M. Walraven, and S. J. J. M. F. Kokkelmans, *Phys. Rev. A* **82**, 042712 (2010).
- [26] K. K. Ni, S. Ospelkaus, D. Wang, G. Quémener, B. Neyenhuis, M. H. G. de Miranda, J. L. Bohn, J. Ye, and D. S. Jin, *Nature* **464**, 1324 (2010).
- [27] G. Quémener and J. L. Bohn, *Phys. Rev. A* **81**, 060701 (2010).
- [28] A. Micheli, Z. Idziaszek, G. Pupillo, M. A. Baranov, P. Zoller, and P. S. Julienne, *Phys. Rev. Lett.* **105**, 073202 (2010).
- [29] M. H. G. de Miranda, A. Chotia, B. Neyenhuis, D. Wang, G. Quémener, S. Ospelkaus, J. L. Bohn, J. Ye, and D. S. Jin, *Nature Phys.* **7**, 502 (2011).
- [30] F. Ferlaino, S. Knoop, M. Berninger, M. Mark, H.-C. Nägerl, and R. Grimm, *Laser Phys.* **20**, 23 (2010).
- [31] The state  $\mu_3$  is difficult to access because of its proximity with  $\mu_4$ .
- [32] Note that this value is two orders of magnitude larger than that of  $p$ -wave dominated fermionic KRb molecules [26].
- [33] G. Quémener, J. L. Bohn, A. Petrov, and S. Kotochigova, *Phys. Rev. A* **84**, 062703 (2011).
- [34] G. Quémener and J. L. Bohn, *Phys. Rev. A* **83**, 012705 (2011).
- [35] M. Greiner, C. A. Regal, and D. S. Jin, *Nature* **426**, 537 (2003).
- [36] S. Jochim, M. Bartenstein, A. Altmeyer, G. Hendl, S. Riedl, C. Chin, J. Hecker Denschlag, and R. Grimm, *Science* **302**, 2101 (2003).
- [37] A. Frisch, K. Aikawa, M. Mark, A. Rietzler, J. Schindler, E. Zupanic, R. Grimm, and F. Ferlaino, *Phys. Rev. A* **85**, 051401(R) (2012).
- [38] G. Quémener, M. Lepers, and O. Dulieu, in preparation (2015).
- [39] Z. Idziaszek and P. S. Julienne, *Phys. Rev. Lett.* **104**, 113202 (2010).
- [40] S. Kotochigova and A. Petrov, *Phys. Chem. Chem. Phys.* **13**, 19165 (2011).

## SUPPLEMENTAL MATERIAL

### Creation of Er<sub>2</sub> in 3D and q2D

We create Feshbach molecules using standard techniques of magneto-association across a Feshbach resonance. As demonstrated in Refs. [12, 13], Er features an enormous number of Feshbach resonances. Here, we focus on the resonances observed below 3 G. In particular, we first create an ultracold atomic sample of about  $3 \times 10^5$  <sup>168</sup>Er atoms at a temperature of  $T \approx 150$  nK, which is just above the onset of Bose condensation, see Ref. [12]. The atoms are confined into a three-dimensional (3D) crossed optical dipole trap with frequencies  $\nu_x = 51.5(2)$  Hz,  $\nu_y = 13.2(3)$  Hz, and  $\nu_z = 207(1)$  Hz. We choose magnetic fields of 1.4 G, 2.3 G, and 2.8 G for the molecular states  $\mu_1$ ,  $\mu_2$ , and  $\mu_4$ , respectively. We then magneto-associate molecules by ramping the magnetic field 150 mG below the Feshbach resonance. The typical ramp speed is 90 mG/ms. After the molecule association, we remove all the residual atoms from the optical dipole trap by applying a short laser pulse. The pulse is on resonance with the strong atomic transition at 401 nm [37] and has a duration of 1  $\mu$ s with an intensity of  $\sim 40$  mW/cm<sup>2</sup>.

To realize a q2D geometry, we superimpose a one-dimensional optical lattice beam to the system after finishing evaporation in the 3D trap. The lattice is realized from a retro-reflected laser beam at 1064 nm, propagating along the vertical direction. The beam has a waist of 250  $\mu$ m and a typical power of 8 W. As a result, the particles are confined into an array of q2D pancakes with frequencies  $\nu_r = 33.0(3)$  Hz in the radial direction and  $\nu_z = 31.2(1)$  kHz in the tightly confining axial direction. We first load the lattice from the atomic sample and we then magneto-associate Er<sub>2</sub> in the lattice. The molecule conversion efficiency in the q2D geometry is  $\lesssim 5\%$ , which is below the one observed in the 3D trap. With this scheme, we produce about  $1.1 \times 10^4$  molecules at a temperature of 400 nK, corresponding to a density of  $3.8 \times 10^7$  cm<sup>-2</sup>. The molecules fill about 35 lattice layers.

We control the molecular dipole orientation by changing the orientation of the magnetic field. The orientation is quantified in term of the angle  $\theta$ , which defines the angle between the quantization axis, set by the magnetic field orientation, and the  $z$ -axis of the lattice trap. We prepare the molecular samples at either  $\theta = 0^\circ$  or  $90^\circ$ , correspondingly side-by-side (repulsive) or head-to-tail (attractive) dipolar collisions. The magnetic field is rotated by using three pairs of independently-controlled magnetic-field coils. We pay particular attention that when changing the orientation of the magnetic field we keep its magnitude constant. We check this by performing radio-frequency spectroscopy between Zeeman sub-levels for different angles of rotation. We typically rotate

the field within  $\sim 6$  ms.

For all our loss-rate measurements, we jump to a magnetic field of about 200 mG after molecule association. At this field,  $E_b$  is of the order of few  $h \times 1$  MHz. We choose to perform our measurement at this magnetic-field value because around 200 mG there are no Feshbach resonances and the molecular spectrum might be less dense. Using a Stern-Gerlach technique [19], we measure  $\mu$  at 200 mG for all the three target molecular states. We find a slight shift of  $\mu$  in comparison with the values from Table I of a few percent to  $10.9(5) \mu_B$  for  $\mu_1$ ,  $11.7(3) \mu_B$  for  $\mu_2$ , and  $8.7(6) \mu_B$  for  $\mu_4$ .

The given uncertainties for the measured loss rates in Table II are composed of a statistical error with one standard deviation derived from fitting a two-body rate equation to the measured data, and a systematic uncertainty coming from number density calibration. Due to the distribution of molecules across many lattice layers this is by far the greatest uncertainty in the q2D geometry. The average 2D density and its uncertainty was calculated using a number-weighted average over occupied lattice layers similar to Ref. [29]. When calculating the loss rate ratio  $\beta_\perp/\beta_\parallel$ , the systematic uncertainty in the density can be neglected as it is highly correlated for the measurement of  $\beta_\perp$  and  $\beta_\parallel$ .

### Collision Formalism

We briefly describe the theoretical formalism used in this article to determine the collisional properties of Er<sub>2</sub> molecules in free space (3D collisions) and in an one-dimensional optical lattice (q2D collisions), in an arbitrary magnetic field  $\vec{B}$ . More details can be found in Ref. [34, 38].

We use a time-independent quantum formalism based on spherical coordinates  $\vec{r} = (r, \theta_r, \phi_r)$  describing the relative motion of two Er<sub>2</sub> molecules. The quantization axis  $\hat{z}$  is chosen to be the confinement axis of the optical lattice. A spherical harmonic basis set, summed over different partial waves  $\ell$  with projections  $m_\ell$  on the quantization axis, is used to expand the total colliding wave function. The one dimensional optical lattice is supposed to be deep enough to consider the collision taking place in an individual pancake. One pancake is represented as an harmonic trap for the relative motion of reduced mass  $m_{\text{red}}$

$$V_{\text{ho}} = \frac{1}{2} m_{\text{red}} \omega^2 z^2 \quad (1)$$

with  $\omega = 2\pi\nu$  and  $\nu = 31.2$  kHz. The 3D collisions are recovered by setting  $\nu = 0$ . We consider molecules in the ground state of the harmonic oscillator. A given state of an Er<sub>2</sub> Feshbach molecule is described by a rather complicated linear combination of atomic states which cannot be precisely calculated as mentioned in the next section

of this Supplemental Material. Therefore we consider that the molecule has a magnetic moment of magnitude  $\mu$  aligned along the magnetic field which makes an angle  $\theta$  with the confinement axis. The interaction between two molecules is provided by the magnetic dipole-dipole interaction

$$V_{\text{dd}} = \frac{\mu^2 (1 - 3 \cos^2(\theta_r - \theta))}{(4\pi/\mu_0) r^3}. \quad (2)$$

We also used an isotropic  $\text{Er}_2 + \text{Er}_2$  van der Waals interaction given by

$$V_{\text{vdW}} = -\frac{C_6}{r^6} \quad (3)$$

with  $C_6 = 4 \times 1760 = 7040$  a.u. which amounts to four times the value of an isotropic atom-atom coefficient of 1760 a.u. from the theoretical work of Ref. [11]. Note that an alternative value of 1723 a.u. based on observed transitions was obtained in Ref. [13]. The Schrödinger equation is solved for each radial intermolecular separations  $r$  using a log-derivative propagation method. Matching the colliding wavefunction and its derivative with appropriate two-dimensional asymptotic boundary conditions at long-range [34] provides the cross section and the rate coefficient as a function of the collision energy for any arbitrary configurations of magnetic fields and confinements. Averaging the cross sections over a 3D and 2D dimensional Maxwell-Boltzmann distribution provides the corresponding thermalized rate coefficients  $\beta(T)$  for a given temperature.

At short range, we assume that the molecules undergo a full loss mechanism process with a unit probability (it can be either an inelastic or a possible reactive process). This assumption, which corresponds to the so-called universal regime in ultracold collisions, considers that the physics is independent of the initial short-range scattering phase-shift [39] of the full potential energy surfaces of  $\text{Er}_4$ . This is what it is usually assumed for theory as nothing is known about this potential energy surface at short range. Then, if the magnitude of the rates differs between experiment and theory, one can learn that an experimental system deviates from this universal regime and short-range effects play a role.

To circumvent this, it is more convenient to compute the ratio of the theoretical rates of two different magnetic field orientations since we will start with the same short-range physics condition for both orientations, and compare it with the corresponding experimental ratio. An analysis based on the universal behavior of dipolar collisions in confinement of Ref. [33] using a Quantum Threshold model leads to the following formula for the ratio  $\beta_{\perp}(T)/\beta_{\parallel}(T)$ . For bosons, using Eq. 30 of Ref. [33] to describe  $\beta_{\perp}$  (dipole dominated) and Eq. 32 of the same reference for  $\beta_{\parallel}$  (confinement dominated) we find

$$\left. \frac{\beta_{\perp}(T)}{\beta_{\parallel}(T)} \right|_{\text{bos}} \sim \left( \frac{a_{\text{dB}}}{a_{\text{ho}}} \right)^4 \frac{a_d}{a_{\text{ho}}} e^{2(a_d/a_{\text{ho}})^{2/5}} \quad (4)$$

when  $a_d, a_{\text{ho}} > a_{\text{vdW}}$  for a fixed value of  $a_{\text{dB}}/a_{\text{ho}}$  where  $a_{\text{dB}}$  is the de Broglie wavelength. For fermions, using Eq. 16 of Ref. [33] to describe  $\beta_{\perp}$  (dipole dominated) and Eq. 14 of the same reference for  $\beta_{\parallel}$  (van der Waals dominated), along with Eq. 27, we find

$$\left. \frac{\beta_{\perp}(T)}{\beta_{\parallel}(T)} \right|_{\text{fer}} \sim \left( \frac{a_d}{a_{\text{vdW}}} \right)^3 \quad (5)$$

when  $a_d, a_{\text{vdW}} < a_{\text{ho}}$ . These formulas suggest to plot the ratio as a function of  $a_d/a_{\text{ho}}$  for bosons for a fixed ratio  $a_{\text{dB}}/a_{\text{ho}} = 2\pi\sqrt{\nu/k_B T}$  and as a function of  $a_d/a_{\text{vdW}}$  for fermions, as it has been done in Fig. 4 for the magnetic polar molecules of  $\text{Er}_2$  and the electric polar molecules of  $\text{KRb}$ .

### Adiabatic Model

In Ref. [13] we presented the theoretical bosonic-erbium Feshbach spectra derived from coupled-channels calculations. We concluded there that such first-principle evaluations can not quantitatively capture the complex scattering behavior of  $\text{Er}$ . In fact with the current computing capabilities, the calculations can not be converged with respect to the number of basis states required to explain the experimental Feshbach-resonance density. For this reason, we developed a novel approach based on adiabatic potentials (adiabats)  $U_n(R; B)$ .

Our adiabatic model starts from the Hamiltonian  $H = -(\hbar^2/2m_r)d^2/dR^2 + V(\vec{R})$ . The first term is the radial kinetic-energy operator with  $\vec{R}$  describing the orientation and the separation between the two atomic dipoles, and  $m_r$  the reduced mass. The second term of the Hamiltonian is the potential operator  $V(\vec{R})$ , which describes the Zeeman and interatomic interactions. It reads  $V(\vec{R}) = \hbar^2 \vec{\ell}^2 / (2m_r R^2) + H_Z + W^{\text{elec}}(\vec{R})$  and incorporates the rotational energy operator with molecular orbital angular momentum  $\ell$ , the Zeeman interaction of two atoms  $H_Z$ , and the electronic potential operator  $W^{\text{elec}}(\vec{R})$  between the particles. Our model assumes that the relative vibrational motion of two  $\text{Er}$  atoms is slow compared to the timescales of the rotational, Zeeman, and “electronic” atom-atom interactions.

The Zeeman interaction is  $H_Z = g\mu_B(j_{1z} + j_{2z})B$ . Here,  $g = 1.16$  is the  $\text{Er}$  g-factor, a magnetic field  $B$  is aligned along the  $\hat{z}$  direction, and  $j_{iz}$  is the  $z$  component of the angular momentum operator  $\vec{j}_i$  of atom  $i = 1, 2$ . The electronic potential operator  $W^{\text{elec}}(\vec{R})$ , described in Refs. [10, 13, 40], is anisotropic, as it depends on the orientation of  $\vec{R}$ . At large separation  $R$ ,  $W^{\text{elec}}(\vec{R})$  is given by the magnetic dipole-dipole interaction plus both the isotropic and anisotropic contribution of the van der Waals interaction. For  $R \rightarrow \infty$  the interaction  $W^{\text{elec}}(\vec{R}) \rightarrow 0$ .

The Hamiltonian is evaluated in the basis  $|a\rangle = |(j_1 j_2) J M\rangle Y_{\ell m_{\ell}}(\hat{R})$ , where  $\vec{J} = \vec{j}_1 + \vec{j}_2$  and  $Y_{\ell m_{\ell}}(\hat{R})$  is



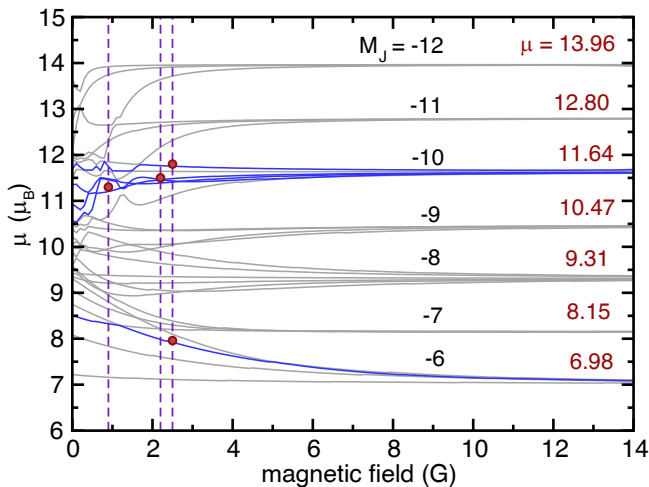


Figure S1. Adiabatic magnetic moment as a function of magnetic field strength evaluated at the entrance channel energy. Each curve corresponds to the adiabatic magnetic moment of one adiabatic potential  $U_n(R; B)$ . The magnetic moments for  $B > 10$  G are given. The dashed vertical lines correspond to the field strength where we have observed a Feshbach resonance. The red-filled circles are the experimentally measured magnetic moments at these resonance locations.

a spherical harmonic. It conserves  $m_\ell + M$  and parity  $p = (-1)^\ell$ . In addition, for bosonic isotopes  $(-1)^{\ell+J} = 1$ . We focus on ultracold collisions between atomic states  $|j_1 m_1\rangle = |j_2 m_2\rangle = |6, -6\rangle$  and, therefore, only include basis functions satisfying  $m_\ell + M = -12$ . We limit the included partial waves to even  $\ell \leq 6$  and thus states with even  $J$ , as the “adiabatic” magnetic moments of the resonances quickly converge with the included number of partial waves. (There is one  $s$ -wave channel in our calculation, four  $d$ -wave channels, eight  $g$ -wave channels, and ....)

The adiabats  $U_n(R; B)$  with  $n = 1, 2, \dots$  are eigenvalues of the operator  $V(\vec{R})$  at a given field strength  $B$ . Their eigenfunctions are  $|n; R\rangle = \sum_a c_{n,a}(R)|a\rangle$  with  $R$ -dependent coefficients  $c_{n,a}(R)$ . Note that we neglect the coupling between  $U_n(R; B)$  due to the radial part of kinetic-energy operator.

Figure 2 shows the adiabats at  $B = 2.44$  G. The scattering starts from the  $s$ -wave entrance channel correlating to the energetically lowest adiabat. All other potentials either have a centrifugal barrier and dissociate to two atoms with  $M = -12$ , or dissociate to closed-channel Zeeman sublevels with  $M > -12$ . Furthermore, the fig-

ure shows that the potentials form energetically distinct groups, where each of the groups can be labeled by a partial wave quantum number. Within a group the potentials are split by the Zeeman energy and the magnetic dipole-dipole interaction.

The adiabatic magnetic moment of a resonance is given by  $\mu_{nv}^{\text{adiab}} \equiv -dE_{nv}(B)/dB \approx -dU_n(R^*; B)/dB$ , where we realize that to good approximation most of the adiabatic vibrational wavefunction is localized around the outer classical turning point. We further note that  $dU_n(R^*; B)/dB = \langle n; R^* | dH_Z/dB | n; R^* \rangle$  from the Hellmann-Feynman theorem and, hence,  $\mu_{nv}^{\text{adiab}} = -g\mu_B \sum_a M_a |c_a(R^*)|^2$ , where  $M_a$  is the total atomic projection quantum number of state  $|a\rangle$ . We assign a resonance by the quantum numbers of the basis state  $|a\rangle$  for which  $|c_a(R^*)|^2$  is largest and note that the absolute value of the magnetic moment of a resonance is always smaller than  $12g\mu_B \approx 14\mu_B$ .

We further assume that the non-adiabatic coupling between the adiabatic potentials is significantly smaller than their spacings for  $R < 100a_0$ . Then a weakly bound level of adiabatic potential  $n$  can lead to a Feshbach resonance when its energy  $E_{nv}(B)$  coincides with the entrance channel energy. The outer turning point  $R^*$  of this level satisfies  $U_n(R; B) = 0$ . The resonance acquires a width due to non-adiabatic coupling to the entrance channel.

Finally, we determine the approximate quantum numbers of experimentally-observed resonances with  $B_{\text{res}} < 3$  G, listed in Table I, based on a comparison of the experimental magnetic moment with those predicted by the adiabatic model at the same resonant field. We find that for these resonances there exist adiabats with a magnetic moment that agrees within 1% uncertainty with the experimental values. A study of the largest coefficients  $c_{n,a}(R)$  at  $R = R^*$  then enables us to assign the dominant quantum states shown in Table I.

Figure S1 shows the magnetic-field dependence of the adiabatic magnetic moment at the entrance channel energy for each of the adiabatic potentials  $U_n(R; B)$ . We see that for  $B > 8$  G the magnetic moment values equal integer multiples of  $g\mu_B$  corresponding to those of the atomic limits. For smaller field strengths the adiabatic magnetic moments show mixing of the Zeeman sublevels. Here, the magnetic moment value depends on the magnetic dipole-dipole interaction but only weakly on the strength and anisotropy of the dispersion potential. The figure also shows our experimentally studied Feshbach resonance locations as well as their magnetic moments  $\mu^{\text{exp}}$ ; see Table I.